A highly efficient solution and solid state ESIPT fluorophore and its OLEDs application

Pei Yu, Virgile Trannoy, Anne Léaustic, Sophie Gadan, Régis Guillot, Clémence Allain, Gilles Clavier, Sandra Mazerat, Bernard Geffroy

NJC

New Journal of Chemistry

A journal for new directions in chemistry

Accepted Manuscript

This article can be cited before page numbers have been issued, to do this please use: P. Yu, V. Trannoy, A. Léaustic, S. Gadan, R. Guillot, C. Allain, G. Clavier, S. Mazerat and B. Geffroy, *New J. Chem.*, 2021, DOI: 10.1039/D0NJ05600F.

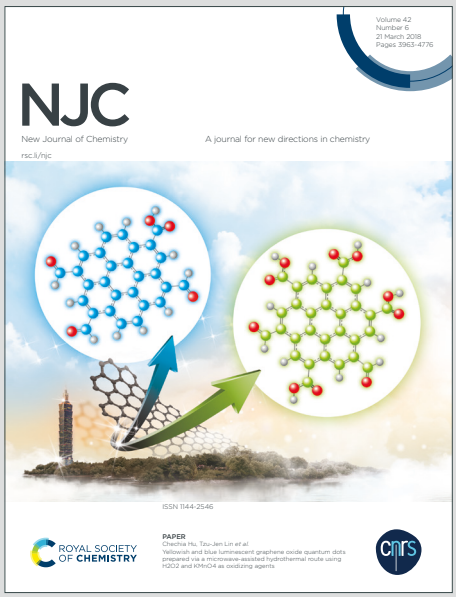

This is an Accepted Manuscript, which has been through the Royal Society of Chemistry peer review process and has been accepted for publication.

Accepted Manuscripts are published online shortly after acceptance, before technical editing, formatting and proof reading. Using this free service, authors can make their results available to the community, in citable form, before we publish the edited article. We will replace this Accepted Manuscript with the edited and formatted Advance Article as soon as it is available.

You can find more information about Accepted Manuscripts in the Information for Authors.

Please note that technical editing may introduce minor changes to the text and/or graphics, which may alter content. The journal's standard Terms & Conditions and the Ethical guidelines still apply. In no event shall the Royal Society of Chemistry be held responsible for any errors or omissions in this Accepted Manuscript or any consequences arising from the use of any information it contains.

Journal Name

ROYAL SOCIETY OF CHEMISTRY View Article Online
DOI: 10.1039/D0NJ05600F

ARTICLE

A highly efficient solution and solid state ESIPT fluorophore and its OLEDs application

Received 00th January 20xx,
Accepted 00th January 20xx

DOI: 10.1039/x0xx00000x

www.rsc.org/

Virgile Trannoy,[ad] Anne Léaustic,[a] Sophie Gadan,[a] Régis Guillot,[a] Clémence Allain,[b] Gilles Clavier,[b] Sandra Mazerat,[a] Bernard Geffroy*[ce] and Pei Yu*[a]

We present herein the synthesis and the photophysics of 2,2'-bipyridine-3,3'-diol-5,5'-dicarboxylic acid ethyl ester ($BP(OH)_2DCEt_2$), an excited state intramolecular proton tranfer (ESIPT)-based fluorophore featuring two identical intramolecular hydrogen bonds. $BP(OH)_2DCEt_2$ emits efficiently not only in solution, including protic solvents (λ_{em} = 521 nm, Φ_f = 40 to 75%), but also in crystalline state (λ_{em} = 530 nm, Φ_f = 51%). In addition, its saponified form ($Na_2BP(OH)_2DC$) is highly fluorescent in water (λ_{em} = 490 nm, Φ_f = 51%). Finally, the good electroluminescence performance of $BP(OH)_2DCEt_2$ is also demonstrated in an OLED device.

Introduction

Organic chromophores with intramolecular hydrogen bond are prone to undergo, upon light absorption, Excited-State Intramolecular Proton-Transfer (ESIPT), an ultrafast photochemical process that leads to a new excited state with an electronic structure quite different from the original one and gives rise thereby to a unique four-level photo-cycle, as illustrated in Scheme 1 in the case of an archetypal molecule of this family, 2-(2-hydroxyphenyl)-benzothiazole (HBT).

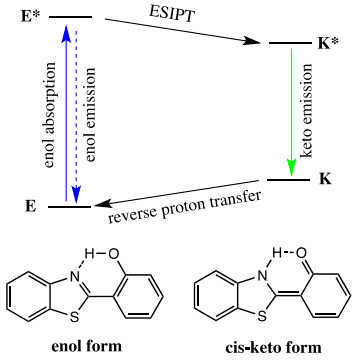

Scheme 1. Four-level photocycle of HBT

As a result, ESIPT chromophores display remarkable fluorescent features, with either a low energy K* emission with large Stokes shift or a dual and tunable E* and K* emission.[1-4] Moreover, unlike most organic fluorophores they also tend to be a more efficient solid state emitter as the self-quenching is minimized due to the absence of spectral overlap between absorption and emission.[5] All these attractive features make ESIPT chromophores prime candidates for various applications such as sensing/imaging,[1,6-11] drug-delivery with real-time fluorescence monitoring,[12] lasing,[1,13-16] OLEDs.[1,17-20] However, ESIPT dyes generally suffer from low emission efficiency, impeding their applications. Synthetic efforts intended to increase their fluorescence quantum yield have mainly focused on 2-(2-hydroxyphenyl)-benzazole scaffold (HBX), such as HBI (X=imidazole), HBO (X=oxazole) and HBT (X=thiazole) and produced some bright ESIPT emitters in solution or/and in solid state.[5,21,22] Nevertheless, their number is quite limited and their quantum yields often low in protic solvents due to competing hydrogen bond formation with the solvents. In this context, design of new ESIPT dyes with high fluorescence efficiency both in solution and in solid state is of high interest for expanding their structural diversity and applications.

Recently, we have prepared and characterized stable, porous and highly fluorescent MIL-140c type MOFs by using a newly designed symmetric ESIPT linker, 2,2'-bipyridine-3,3'-diol-5,5'-dicarboxylic acid ($H_2BP(OH)_2DC$, Scheme 2).[23]

[a] Université Paris-Saclay, CNRS, Institut de Chimie Moléculaire et des Matériaux d'Orsay, 91405, Orsay, France.
[b] Université Paris-Saclay, ENS Paris-Saclay, CNRS, PPSM, 91190 Gif-sur-Yvette, France.
[c] Université Paris-Saclay, CEA, CNRS, NIMBE, LICSEN, 91191, Gif-sur-Yvette, France.
[d] Present address : Instituto de Ciencia Molecular (ICMol), Universidad de Valencia, c/ Catedratico José Beltran 2, 46980 Paterna, Spain.
[e] LPICM, CNRS, Ecole Polytechnique, Institut Polytechnique de Paris, route de Saclay, 91128 Palaiseau, France.

Electronic Supplementary Information (ESI) available: Detailed X-Ray crystallographic data (CCDC 2004784), ^{1}H NMR, ^{13}C NMR and fluorescence spectra and AFM images. See DOI: 10.1039/x0xx00000x

View Article Online
DOI: 10.1039/D0NJ05905E

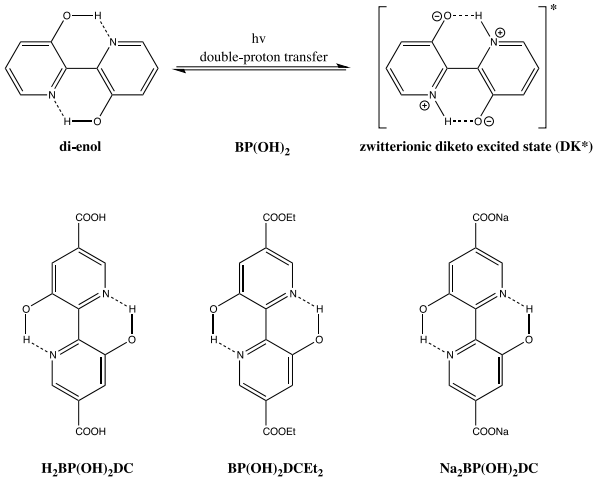

Scheme 2. $BP(OH)_2$ with its ground and emitting state (top); $BP(OH)_2DCEt_2$, its diacid and disodium forms (bottom)

The target linker derives from 2,2'-bipyridine-3,3'-diol ($BP(OH)_2$, Scheme 2), a molecule featuring two intramolecular hydrogen bonds and well-documented for its intense double-proton-transfer based fluorescence and applications.[24-32] More importantly, even in protic solvents such as MeOH and EtOH, where most ESIPT dyes are not or only weakly fluorescent, $BP(OH)_2$ keeps a more than decent quantum yield of 10 and 18%, respectively.[26] However, to our surprise, very few fluorescent derivatives of $BP(OH)_2$ have been reported in the literature.[33-38] In this work, we report the synthesis, crystal structure and photophysics of a highly fluorescent and functionalized $BP(OH)_2$ derivative, namely 2,2'-bipyridine-3,3'-diol-5,5'-dicarboxylic acid ethyl ester ($BP(OH)_2DCEt_2$, (Scheme 2), precursor of $H_2BP(OH)_2DC$. The new compound substantially outperforms the parent $BP(OH)_2$ in solution, including in protic solvents, and emits efficiently in crystalline state. Finally, good electroluminescence performance of $BP(OH)_2DCEt_2$ is also demonstrated in an OLEDs device.

Results and discussion

Synthesis and characterizations

Starting from the commercially available 5-hydroxy-3-pyridinecarboxylate $BP(OH)_2DCEt_2$ was synthesized according to Scheme 3 in three straightforward steps with good overall yield.

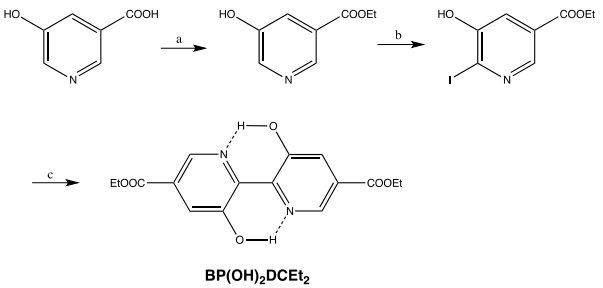

Scheme 3. Synthetic route of $BP(OH)_2DCEt_2$: a) EtOH, $SOCl_2$/reflux; b) Aqueous Na_2CO_3, I_2 at RT; c) Zn, LiCl, $NiCl_2.6H_20$ (cat) /DMF at RT and then at 50°C.

Adapting a phosphine-free nickel catalytic system reported for the synthesis of symmetric and dissymmetric bipyridines,[39] 5-hydroxy-6-iodo-niconic acid ethyl ester was reductively homo-coupled to give $BP(OH)_2DCEt_2$ in good yield. $BP(OH)_2DCEt_2$ was fully characterized by standard techniques as well as by single crystal analyses (more details can be found in the ESI). The molecule crystallizes in *C2/c* space group, with its molecular structure shown in Figure 1.

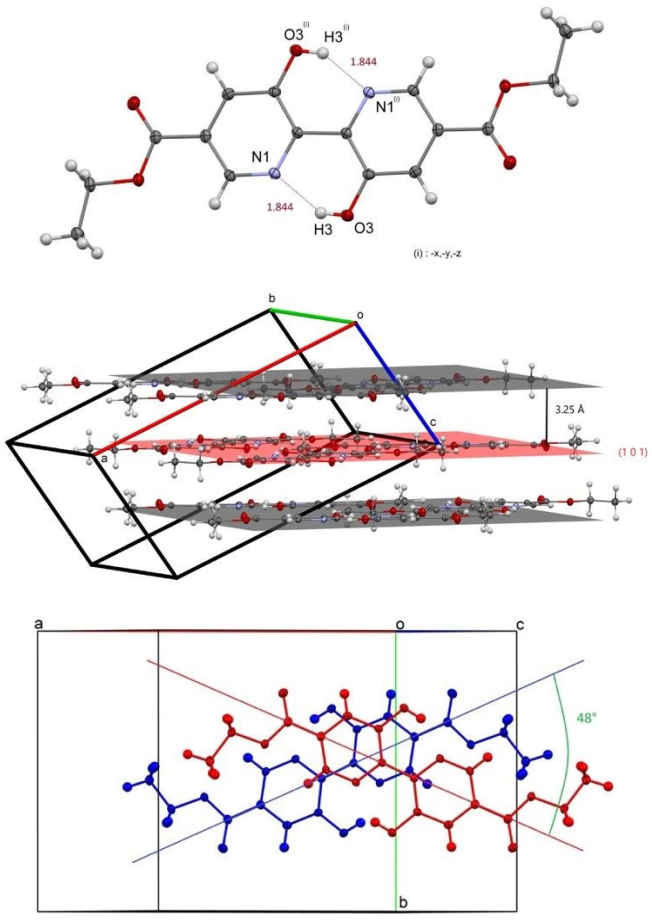

Figure 1. Molecular structure of $BP(OH)_2DCEt_2$ (top); π stacking (middle); angle between the long axis of two adjacent stacked molecules (bottom).

Like the parent $BP(OH)_2$ and its 6,6'-dimethyl substituted derivative,[40,41] $BP(OH)_2DCEt_2$ adopts a planar geometry due to the two strong and identical hydrogen bonds between the two pyridinic rings of the central $BP(OH)_2$ moiety (Figure 1, top). On the other hand, there is no intermolecular hydrogen bonding nor other close contacts between adjacent molecules except a significant π stacking that runs along the [101] crystallographic direction, with a mean interlayer distance of ca. 3.25 Å (Figure 1, middle). Note that the two adjacent molecules are not co-facial but more in a slip-stacking mode with, moreover, an angle of 48° between the long axis of the molecules (Figure 1, bottom).

Fluorescence

IN ORGANIC SOLVENTS. The emission properties of $BP(OH)_2DCEt_2$ were investigated by steady-state fluorescence at room temperature in four different and aerated solvents. Its

View Article Online
DOI: 10.1039/D0NJ05600F

absorption and emission spectra are shown in Figure 2 and the main spectroscopic data listed in Table 1 along with available data of $BP(OH)_2$ for comparison.

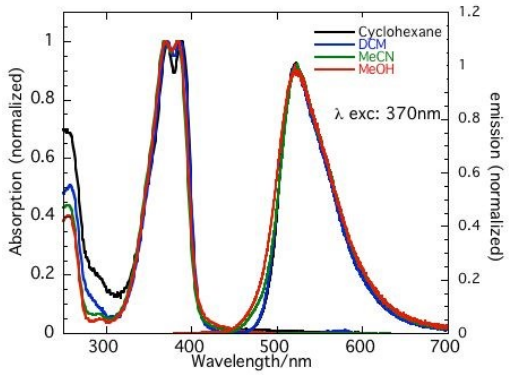

Figure 2. Normalized absorption and emission spectra of $BP(OH)_2DCEt_2$ in different solvents.

Table 1. Photophysical data of $BP(OH)_2DCEt_2$, $Na_2BP(OH)_2DC$ and $BP(OH)_2$ in different solvents.

	Solv.	λ_{ab} (nm)	ε ($M^{-1}.cm^{-1}$)	λ_{em} (nm)	Φ_F
$BP(OH)_2DCEt_2$	C_6H_{12}	372, 389		521	0.70
	CH_2Cl_2	372, 388	15900	521	0.75
	MeCN	370, 385		521	0.57
	MeOH	370, 385		521	0.40
	H_2O+dmso(3%)	370, 385		540	0.29
$BP(OH)_2$	C_6H_{12}	340-350		500	0.31[a]
	CH_2Cl_2	340-350		500	0.21[b]
	MeCN	340-350		500	0.09[c]
	MeOH	340-350		480	0.10[c]
	H_2O	347, 403, 430		460	0.04[c]
$Na_2BP(OH)_2DC$	H_2O	360, 426, 460		490	0.51

[a] Ref. 24; [b] Ref. 27; [c] Ref. 26

$BP(OH)_2DCEt_2$ mainly absorbs in the UV region, with a strong and rather structured low energy band located between 370-385 nm, while its emission is broad and centred at 521 nm. Both the absorption and emission spectra only slightly vary with solvents of different polarity and proticity.

In comparison with $BP(OH)_2$, the major difference in absorption is a redshift of ca. 30 nm for the low energy band likely due to a more stabilized LUMO by the electron-withdrawing ester groups, while its emission is red-shifted by ca. 20 nm in aprotic solvents and ca. 40 nm in protic solvents like MeOH (Table 1). However, the most remarkable difference between the two is the quantum yield of emission. The new emitter has a much higher efficiency in all solvents investigated (Table 1). Particularly noteworthy is the still high quantum yield of 40% in methanol, which is four times that reported for $BP(OH)_2$.[26] The emission was also studied by time-resolved fluorescence emission in dichloromethane. A single-exponential decay was observed with a fluorescence lifetime of 4.64 ns, which is superior to that of 3.2 ns reported for $BP(OH)_2$ in the same solvent.[27] This emission is not sensitive to oxygen as the same decay was obtained in degassed dichloromethane.

The reasons to such an enhancement in the fluorescence efficiency are not yet clear. Due to the presence of electron-accepting ester group one could expect significant changes in the strength of the intramolecular hydrogen bond, which directly affects the ESIPT process and its emission. Actually, the measured chemical shift of the hydrogen atom engaged in the hydrogen bond (δ=14.40 ppm) is very close to that reported for $BP(OH)_2$ (δ=14.54 ppm),[35] indicating therefore a very similar strength of the intramolecular hydrogen bonds within the two fluorophores. This unusually small substitution effect is however not unexpected since the enhancement of the hydrogen donating ability of the hydroxyl group is offset at least in part by a concomitant decrease in the hydrogen accepting capability of the nitrogen atom located on the same ring, leading thus to an overall limited impact on the hydrogen bonding in symmetrically substituted $BP(OH)_2$ derivatives.

One possible explanation to the observed fluorescence enhancement could be a better "insulation" of the emitting state from the solvent in $BP(OH)_2DCEt_2$ than in $BP(OH)_2$. And this is best reflected in methanol where a blue shift in emission, observed for $BP(OH)_2$ (Table 1), is thought to be related to some specific interactions of its excited state (DK*, Scheme 2) through formation of intermolecular hydrogen bonds with protic solvents,[27,29] while this is not the case for $BP(OH)_2DCEt_2$ (Table 1) probably due to a different pattern of intermolecular interactions between $BP(OH)_2DCEt_2$ and solvent molecules.

IN WATER. ESIPT dyes are generally not or only weakly fluorescent in water as the intramolecular hydrogen bond of the dye, mandatory for the ESIPT process, is disrupted or at least weakened to a large extent by formation of intermolecular hydrogen bonds. The high quantum yield of $BP(OH)_2DCEt_2$ in methanol suggests a better ESIPT emitter in water than the weakly fluorescent $BP(OH)_2$.[26]

$BP(OH)_2DCEt_2$ being insoluble in water, dimethyl sulfoxide (DMSO) was used as co-solvent (3% in volume) to prepare an aqueous solution of the dye for fluorescence characterizations. To our delight, the solution remains highly fluorescent, with a slightly redshifted maximum at 540 nm and a measured quantum yield still up to 29% (Table 1). In addition, even if it is expected for ESIPT dyes, the high quantum yield makes the new emitter potential candidate as a sensitive pH probe. As a matter of fact, the fluorescence underwent drastic changes when the pH was gradually brought from 6 to 12 (Figure S1), while the emission colour changed from yellow-green to blue-cyan. Such changes are clearly associated with a progressive deprotonation of the two OH functions of $BP(OH)_2DCEt_2$. Using global analysis (ReactLab™-EQUILIBRIA) the fluorescence responses could be satisfactorily fitted with two proton dissociation constants of pKa = 8.1 and 11.3, respectively. These pKa values are smaller than those (9.2, 12.4) reported for $BP(OH)_2$,[27] but consistent with the expected electron-withdrawing effect of ethyl ester group.

The dicarboxylic acid form of the new emitter, $H_2BP(OH)_2DC$ (Scheme 2), is not sufficiently soluble in water for fluorescence measurements. This very low solubility can probably be attributed to the presence of multiple strong

View Article Online DOI: 10.1039/D0NJ05600B

intermolecular hydrogen bonds between neighbouring molecules in the solid state. However, its disodium dicarboxylate form ($Na_2BP(OH)_2DC$, Scheme 2) is pretty soluble in water owing to its twice negatively charged nature at neutral pH. Its absorption and emission spectra are shown in Figure 3.

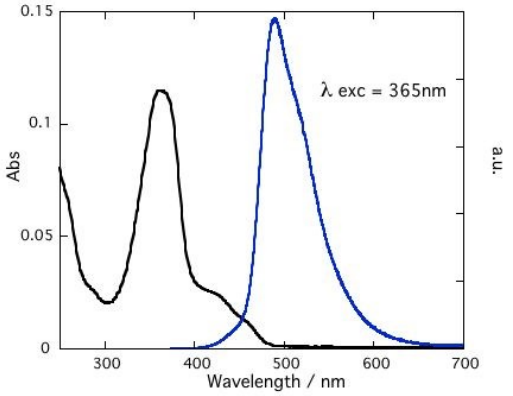

Figure 3. Absorption and emission spectrum of $Na_2BP(OH)_2DC$ in water ($6\ 10^{-6}$ M) at 25°C.

The absorption spectrum of $Na_2BP(OH)_2DC$ in water is characterized by an intense band at 360 nm and two others of much lower intensity located between 400 and 480 nm (Table 1). This spectrum resembles qualitatively that of $BP(OH)_2$ in water[27,29] and by analogy, the two bands at lower energy can be reasonably assigned to the zwitterionic diketo form stabilized in the ground state by formation of intermolecular hydrogen bonds with water molecules.

The emission of $Na_2BP(OH)_2DC$ peaks at 490 nm and represents a redshift of ca. 30 nm in comparison with that of $BP(OH)_2$ (Table 1). But the most remarkable feature of this ESIPT emission is its quantum yield of 51%, which is more than ten times that of $BP(OH)_2$ in water.[26]

Like $BP(OH)_2DCEt_2$, the fluorescence of $Na_2BP(OH)_2DC$ is particularly sensitive to the pH of the solution, as shown in Figure 4.

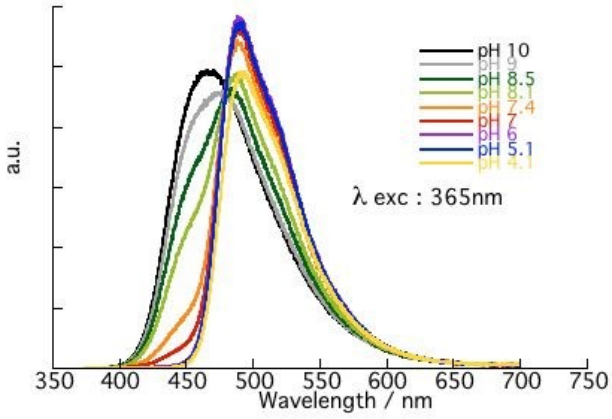

Figure 4. Fluorescence changes of $Na_2BP(OH)_2DC$ versus pH in water at 25°C

In the pH range between 7 and 10, the observed changes in fluorescence are linked to the progressive deprotonation of the two OH functions and suggest the generation of a new blue emitting species, corresponding probably to the triple negatively charged species after first proton removal. While the rapid decrease in intensity of the initial fluorescence when lowering pH below 5 is likely due to the combination of two effects: 1) partial breakdown of the intramolecular hydrogen-bonds; 2) the formation of the scarcely water-soluble dicarboxylic form, $H_2BP(OH)_2DC$. Finally, analysis of the fluorescence response vs pH in the range from 5 to 10 allowed to determine the first proton dissociation constant (pKa) of the two OH functions to be 8.0, similar to what is obtained for the ester derivative $BP(OH)_2DCEt_2$.

In Crystalline State. The emission of $BP(OH)_2DCEt_2$ in solid state was investigated at room temperature by both steady-state fluorescence spectroscopy with an integrating sphere and time-resolved fluorescence.

The emission spectrum of the pristine microcrystals is qualitatively very close to that in solution, with a maximum centred around 530 nm and a measured quantum yield of 51% (Figure S2). Then the decay was monitored by time-resolved fluorescence at three different wavelengths of the emission: 510 nm (blue-edge), 530 nm (maximum) and 580 nm (red-edge). The three decays could be well fitted using a two-exponential model with decay times of 2.06 ns and 4.74 ns. The long decay time, making up to ca. 95% of the total fluorescence, is very close to the fluorescence lifetime measured in dichloromethane (4.64 ns), while the short decay (ca. 5%) could likely be ascribed to the surface and near-surface molecules in the microcrystals which experience a different environment. Comparison of the decays at different emission wavelengths shows that the relative contributions of the two decay times to the overall fluorescence only slightly vary with the emission wavelength, which indicate that there are no excited-state processes such as excimers or resonance energy transfer occurring in the solid.

The high solid-state quantum yield, comparable to those in solution, is clearly due to the absence of the so called "Aggregation Caused Quenching" (ACQ), generally encountered in solid state for organic dyes. Two reasons can be put forward. Firstly, resonance energy transfer, one of the main contributors to ACQ, is suppressed due to the absence of spectral overlap between the absorption and emission of the dye. Secondly, the crystal structure has favourable intermolecular arrangements (Figure 1). Indeed, the only significant intermolecular interactions are between molecules involved in a kind of π slip-stacking, which is believed to enhance solid state emission.[1]

Electroluminescence

The electroluminescence properties of $BP(OH)_2DCEt_2$ was investigated to access its potential as emitting dye in OLEDs device whose structure is shown in Scheme 4. The emitting layer (EML) is $BP(OH)_2DCEt_2$ molecules either as neat film or host-guest system of 20 nm thick (See experimental for details of OLED fabrication and characterization).

View Article Online
DOI: 10.1039/D0NJ05600F

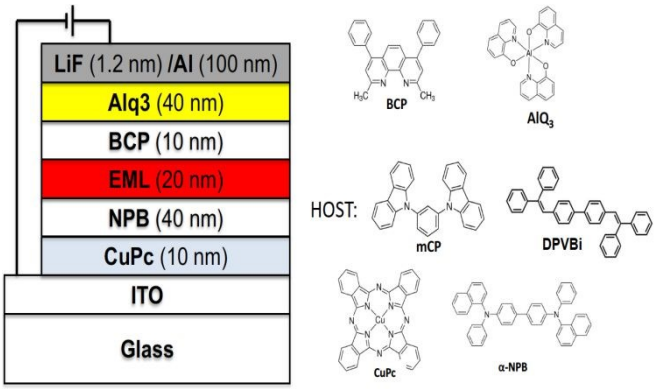

Scheme 4. OLED device structure and molecular materials used.

The solid-state photoluminescence yields (PL) of the emitting layer are given in Table 2 and the PL spectrum is shown in Figure 5 for a 70 nm thick neat film. The PL emission peak is centred at 536 nm with a FWHM around 60 nm. The PL yields of the neat films are very high (~80 %) showing the interest of $BP(OH)_2DCEt_2$ molecule for OLEDs fabrication. For the guest-host films, the PL yield increases with the concentration of the $BP(OH)_2DCEt_2$ molecule in the host and particularly with mCP as host material. For 10% doping ratio, PL efficiency is higher for mCP than for DPVBi used as host. This could be explained by self-absorption or the particular morphology of the film as discussed below.

Table 2. Thin film PL efficiency

Host	Doping ratio (%)	Film thickness (nm)	PL yield[a] (%)
no	100	20	77
	100	70	85
mCP	1.5	20	22
	4	20	20
	10	20	54
DPVBi	0.7	20	25
	4	20	31
	8	20	35
	10	20	32

[a]PL measurement accuracy is 10%

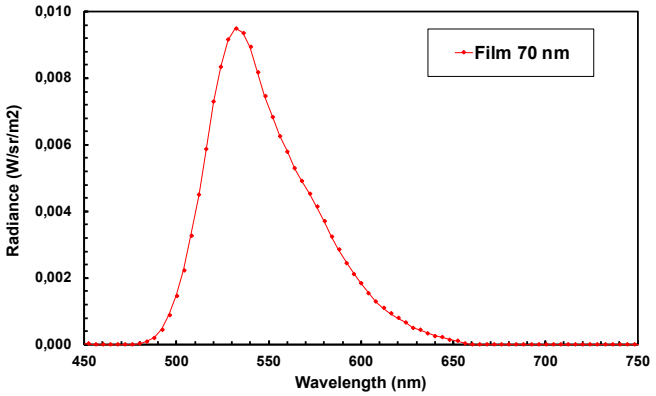

Figure 5. PL spectrum of a neat film of 70 nm thick (excitation at 405 nm)

The electroluminescence (EL) performance of the OLED devices are reported in Table 3 for the neat film and for the guest-host systems as a function of the host material and the doping ratio and the EL spectra are shown in Figure 6.

Table 3. OLEDs devices performances.

Host	Doping ratio (%)	EQE[a] (%)	cd/A[a]	lm/W[a]	EL peak (nm)	Luminance[b] (cd/m²)	CIE chromaticity[b] (x;y)
No	100	-	-	-	-	-	-
mCP	1.5	1.4	5.3	1.7	540	1422	0.336; 0.592
	4	1.5	5.1	1.7	540	1515	0.346; 0.600
	10	1.5	5.3	1.7	540	1510	0.347; 0.600
DPVBi	0.7	1.7	5.4	1.6	532	1571	0.304; 0.554
	1.4	2.3	7.5	2.6	536	2206	0.325; 0.569
	1.8	2.2	7.2	2.6	536	2104	0.318; 0.577
	4	1.8	6.0	2.0	536	1819	0.335; 0.593
	5.6	1.3	4.6	1.2	540	1260	0.342; 0.588
	8	-	-	-	-	-	-
	10	-	-	-	-	-	-

[a] recorded at 10 mA/cm², [b] recorded at 30 mA/cm², error bar ± 10 %, - not measurable.

View Article Online
DOI: 10.1039/D0NJ05600F

Journal Name

ARTICLE

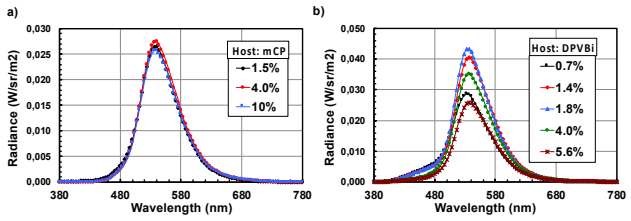

Figure 6. EL spectra recorded at 30 mA/cm². a) mCP as host material, b) DPVBi as host material.

The EL spectra are similar to the PL spectrum of the neat film (Figure 5) showing that the EL emission is due to $BP(OH)_2DCEt_2$ molecule. For the neat film (100 % doping ratio), the devices show a short-circuit and therefore no light is emitted. This result is explained by the crystallization of $BP(OH)_2DCEt_2$ molecules after evaporation, as revealed by AFM (Figure S3), and the diffusion of aluminum electrode through the layer. When mCP is used as host, the EL device characteristics are almost constant from a doping ratio of 1.5% to 10%. The external quantum efficiency (EQE), luminous efficiency (cd/A) and power efficiency (lm/W) are 1.5 ± 0.2 %, 5.3 ± 0.5 cd/A and 1.7 ± 0.2 lm/W respectively. As shown in Figure 6a, the EL emission is from $BP(OH)_2DCEt_2$ molecule with a complete transfer from the host to the guest and the emission peak position is stable at 540 nm. The CIE chromaticity coordinates are slightly shifted by increasing of the doping ratio.

For DPVBi used as host the results are different as reported in Table 3 and Figure 6b. The device performances are dependent of the doping rate with a maximum efficiency reached for a doping ratio of 1.4 - 1.8 %. For low doping ratio (< 1.8 %), the device efficiency is improved by increasing the doping ratio and the EL emission peak is shifted from 532 to 536 nm. As shown in Figure 6b, the exciton transfer from the DPVBi host to the guest molecule is not complete for such low doping ratios and some light is coming from the DPVBi layer in the 430 – 480 nm range. For a doping ratio > 1.8 %, the device performances decreased until a doping ratio of 8 % where no EL emission is obtained. Note that for a doping ratio of 5.6 %, the EL peak is at the same position as for the mCP host and the CIE coordinates have almost reached the ones with mCP host. Surprisingly, the EL emission stopped for a doping ratio of 8 % and 10 % and the devices are short-circuited similarly to the results reported previously for the neat emitting layer. By increasing the doping ratio up to 8 %, the guest-host system tends to crystallize like for the neat film (Figure S4). For the best device (1.4 – 1.8 % doping ratio range), EQE, cd/A and lm/W are 2.3 ± 0.2 %, 7.5 ± 0.5 cd/A and 2.6 ± 0.2 lm/W respectively. As shown in Figure 7, the luminous efficiency is almost constant as a function of the current density and the luminance is well proportional to the current density. A luminous efficiency of 7.5 cd/A is a very good value for a pure fluorescent emitter.

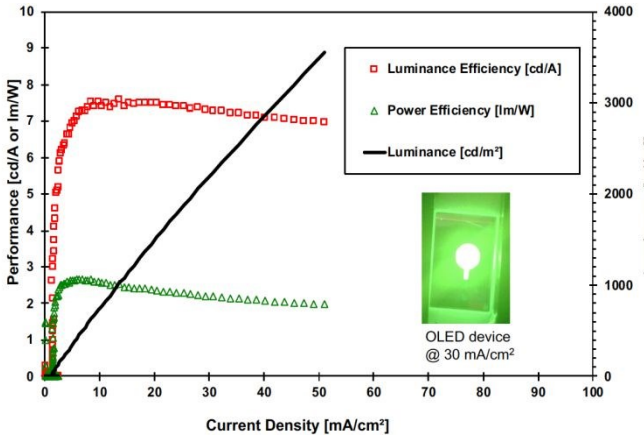

Figure 7. EL performance of the DPVBi: 1.4 % $BP(OH)_2DCEt_2$ OLED device. Insert shows a photograph of the OLEDs device recorded at a current density of 30 mA/cm².

Conclusions

In summary, we have designed and fully characterized a new ESIPT emitter derived from the well-known $BP(OH)_2$. It is found to be a robust ESIPT emitter in all solvents investigated, including protic ones, with fluorescence quantum yields exceeding by far those of $BP(OH)_2$. More interestingly, its dicarboxylate form fluoresces efficiently in pure water with a quantum yield up to 51%, and this fluorescence is highly pH dependent. In crystalline state, it is also found to be an excellent ESIPT emitter and performs quite decently as a pure fluorescent emitter in an OLED device. Of course, its EQE is far below the state of the art, but recent studies show that much higher EQE could be achieved with ESIPT chromophores displaying TADF (Thermally Activated Delayed Fluorescence) properties.[18,19] Finally, with two ester functions that can be easily further derivatized the new emitter constitutes an appealing and versatile entrance for the design of novel luminescent systems.

Experimental

General: Solvents and reagents are used as received unless otherwise stated. Elemental analyses were performed by Service de Microanalyse, ICSN, 91198, Gif sur Yvette,

France. Fluorescence spectra were recorded either on a Fluromax-4 or a Fluorolog spectrometer (Horiba Jobin Yvon). Fluorescence quantum yield in solution were determined using 9,10-diphenylanthracene in cyclohexane as reference ($\Phi = 0.9$). Absolute fluorescence quantum yields of crystalline $BP(OH)_2DCEt_2$ were measured using a Quanta-Phi integrating sphere (Horiba Jobin Yvon). Fluorescence decay curves were obtained by the time-correlated single-photon counting (TCSPC) method with a femto-second laser excitation composed of a Titanium Sapphire laser (Tsunami, Spectra-Physics) pumped by a doubled Nd:YVO_4 laser (Millennia Xs, Spectra-Physics). Light pulses at 800 nm from the oscillator were selected by an acousto-optic crystal at a repetition rate of 4 MHz, and then doubled at 400 nm by a nonlinear crystal. Fluorescence photons were detected at 90° through a monochromator and a polarizer at magic angle by means of a Hamamatsu MCPR3809U photomultiplier, connected to a SPC-630 TCSPC module from Becker & Hickl. The instrumental response function was recorded before each decay measurement with a FWHM (full width at half-maximum) of ~25 ps. The fluorescence data were analyzed using the Globals software package developed at the Laboratory for Fluorescence Dynamics at the University of California, Irvine, which includes reconvolution analysis and global nonlinear least-squares minimization method. UV-Vis absorption spectra were recorded on a Varian Cary 5000 spectrometer equipped with a temperature control unit.

Syntheses

The commercially available but quite expensive ethyl 5-hydroxy-3-pyridinecarboxylate and ethyl 5-hydroxy-6-iodo-3-pyridinecaroxylate can be readily prepared from the much cheaper corresponding acid and used without chromatographic purifications for the synthesis of $BP(OH)_2DCEt_2$ as follows.

Ethyl 5-hydroxy-3-pyridinecarboxylate: to a mixture of 5-hydroxy-3-pyridinecarboxylic acid (5.00 g, 36 mmol) in absolute ethanol (100 ml) cooled at 0° C was added dropwise thionyl chloride (10.5 ml, 72 mmol). The mixture was left to warm up to room temperature and refluxed overnight. After removal of the solvent under reduced pressure the residue was dissolved in water (100 ml) and pH of the solution was adjusted to 7 by cautious addition of solid sodium hydrocarbonate in small portions. After filtration, washing with water the title compound was obtained as an off-white microcrystalline solid and used for the next step without further purification (5.0 g, 83% yield). ^{1}H NMR ($CDCl_3$, 7.26 ppm): δ = 8.77 (s, 1H), 8.46 (s, 1H), 7.90 (s, 1H), 4.41 (q, ^{3}J = 7.3 Hz, 2H) and 1.41 (t, ^{3}J = 7.3 Hz, 3H).

Ethyl 5-hydroxy-6-iodo-3-pyridinecaroxylate: ethyl 5-hydroxy-3-pyridinecarboxylate (5.00 g, 30 mmol), sodium carbonate (6.36 g, 60 mmol) and iodine (7.61 g, 30 mmol) in water (200 mL) were stirred vigorously at room temperature overnight. The pH of the orange solution was then adjusted to ca 7 with hydrochloric acid (1M) and the resulting beige microcrystalline precipitate was filtered, washed with water and dried under vacuum, affording the title compound (7.30 g, 83% yield). ^{1}H NMR ($CDCl_3$): δ = 8.56 (d, ^{4}J = 1.9 Hz, 1H), 7.75 (d, ^{4}J = 1.9 Hz, 1H), 5.87 (bs, 1H), 4.40 (q, ^{3}J = 7.0 Hz, 2H) and 1.40 (t, ^{3}J = 7.0 Hz, 3H).

$BP(OH)_2DCEt_2$: ethyl 5-hydroxy-6-iodo-3-pyridinecarboxylate (2.93 g, 10 mmol), LiCl (0.43 g, 10 mmol) and $NiCl_2.6H_2O$ (0.24 g, 1.0 mmol) were dissolved in DMF (20 ml). To the resulting blue solution was added zinc dust (0.78 g, 12 mmol) and the mixture was stirred at room temperature under argon. After few minutes the mixture turned deep red with concomitant rise of temperature to 40-50 °C. Once subsided, the stirring continued for 1h at RT and 1h at 50-55 °C to ensure the completion of the reaction. The cooled mixture was made acidic (pH = 1 to 2) with aqueous HCl (~1M) and the mixture vigorously stirred 30 min. before the pH was brought back to ca. 4 with solid $NaHCO_3$. CH_2Cl_2 (100 ml) was added and the organic phase collected. The aqueous phase was extracted with CH_2Cl_2 (3x30 ml) and the combined organic phase was dried over Na_2SO_4 and concentrated. The residue was subjected to column chromatography (silica gel, CH_2Cl_2) to afford the title compound as brilliant yellow microcrystalline solid (1.215 g, 73%). ^{1}H NMR ($CDCl_3$): δ = 14.40 (s, 2H), 8.70 (d, ^{4}J = 1.8 Hz, 2H), 8.03, ^{4}J = 1.8 Hz, 2H), 4.44 (q, ^{3}J = 7.0 Hz, 4H), 1.42 (t, ^{3}J = 7.0 Hz, 6H). ^{13}C NMR ($CDCl_3$, 77 ppm): 164.3, 156.2, 141.7, 137.6, 128.1, 127.0, 61.8, 14.3. HRMS (ESI): $C_{16}H_{16}N_2O_6$ found: 331.0931[M-H]$^-$, calculated: 331.0936. Elemental analysis calculated (%) for $C_{16}H_{16}N_2O_6$: C 57.83, H 4.85, N 8.43; found: C 57.87, H 4.93, N 8.35.

Single crystals suitable for structure determination were grown by slow evaporation of $BP(OH)_2DCEt_2$ in a mixture of CH_2Cl_2 and MeCN at room temperature.

OLEDs device fabrication and characterization

The OLED devices were fabricated onto indium tin oxide (ITO) glass substrates purchased from Xin Yang Technology (90 nm thick, sheet resistance of 15 Ω/□). Prior to organic layer deposition, the ITO substrates were cleaned by sonication in a detergent solution, rinsed twice in de-ionized water and then in isopropanol solution and finally treated with UV-ozone during 15 minutes. The OLEDs stack used in this study is the following: Glass / ITO / CuPc (10 nm) / α-NPB (40 nm) / EML 20 nm / BCP (10 nm) / Alq3 (40 nm) / LiF (1.2 nm) / Al (100 nm). Copper II phthalocyanine (CuPc) is used as hole injection layer (HIL), N, N'-Bis-(1-naphthalenyl)- N,N'-bis-phenyl-(1,1′-biphenyl)-4,4′-diamine (αNPB) as hole transport layer (HTL), bathocuproine (BCP) as hole blocking layer (HBL), tris-(8-hydroxyquinoline)aluminum (Alq_3) as electron transport layer (ETL), lithium fluoride as electron injection layer (EIL) and 100 nm of aluminum as the cathode, respectively. The architecture of the device as well as the molecular structure of the materials are shown in Scheme 4. The emitting layer (EML) is $BP(OH)_2DCEt_2$ molecule either as a neat film or a host-guest system of 20 nm thick. The material used as host is 1,3-Bis(*N*-carbazolyl)benzene (mCP) and 4,4′-bis(2,2-

diphenylvinyl)-1,1′-biphenyl, (DPVBi). $BP(OH)_2DCEt_2$ is used as guest with a doping ratio of 0.7 to 10 % weight in the guest-host EML. All the organic materials were purchased from commercial companies except for the $BP(OH)_2DCEt_2$ molecule. Organic layers were sequentially deposited onto the ITO substrate at a rate of 0.2 nm/s under high vacuum (10^{-7} mbar). The doping rate was controlled by simultaneous co-evaporation of the host and the dopant. An in-situ quartz crystal was used to monitor the thickness of the layer depositions with an accuracy of 5%. The active area of the devices defined by the Al cathode was 0.3 cm^2. The organic layers and the LiF/Al cathode were deposited in a one-step process without breaking the vacuum.

After deposition, all the measurements were performed at room temperature and under ambient atmosphere with no further encapsulation of devices. The current–voltage–luminance (I–V–L) characteristics of the devices were measured with a regulated power supply (ACT100 Fontaine) combined with a multimeter (Keithley) and a 1 cm^2 area silicon calibrated photodiode (Hamamatsu). Electroluminescence (EL) spectra and chromaticity coordinates of the devices were recorded with a PR650 SpectraScan spectrophotometer, with a spectral resolution of 4 nm. Photoluminescence (PL) properties of the EML layer are obtained at room temperature with an integrating sphere (LabSphere) and illumination with a 405 nm laser diode. For PL measurements, the films were deposited on pre-cleaned glass substrates in the same deposition sequence as for the OLED devices.

Conflicts of interest

There are no conflicts to declare.

Acknowledgements

We acknowledge the LabEx CHARMMMAT (ANR-11-LABX-0039) for the postdoctoral fellowship of Virgile Trannoy. Arnaud Brosseau (PPSM) is gratefully acknowledged for his help with the time-resolved fluorescence measurements.

References

1 J. E. Kwon and S. Y. Park, *Adv. Mater*., 2011, **23**, 3615.
2 J. Zhao, S. Ji, Y. Chen, H. Guo and P. Yang, *Phys. Chem. Chem. Phys*., 2012, **14**, 8803.
3 A. P. Demchenko, K-C. Tang and P-T. Chou, *Chem. Soc. Rev*., 2013, **42**, 1379.
4 C-L. Chen, Y-T. Chen, A. P. Demchenko and P-T. Chou, *Nat. Rev. Chem*. 2018, **2**, 131.
5 V. S. Padalkar and S. Seki, *Chem. Soc. Rev*., 2016, **45**, 169.
6 A. C. Sedgwick, L. Wu, H-H. Han, S. D. Bull, X-P. He, T. D. James, J. L. Sessler, B. Z. Tang, H. Tian and J. Yoon, *Chem. Soc. Rev*., 2018, **47**, 8842.
7 L. Wu, A. C. Sedgwick, X. Sun, S. D. Bull, X-P. He and T. D. James, *Acc. Chem. Res*. 2019**, 52**, 2582.
8 P. Zhang, C. Fu, Q. Zhang, S. Li and C. Ding, *Anal. Chem*. 2019, **91**, 12377.
9 Y. Zhang, H. Yang, H. Ma, G. Bian, Q. Zang, J. Sun, C. Zhang, Z. An and W-Y. Wong, *Angew. Chem. Int. Ed*. 2019, **58**, 8773.
10 Y. Wu, Z. Li and Y. Shen, *Acs Omega*, 2019, **4**, 16242.
11 D. Dahal, S. Pokhrel, L. McDonald, K. Bertman, S. Paruchuri, M. Konopka and Y. Pang, *ACS Appl. Bio. Mater*. 2019, **2**, 4037.
12 a) S. Barman, S. K. Mukhopadhyay, S. Biswas, S. Nandi, M. Gangopadhyay, S. Dey, A. Anoop and N. D. P. Singh, *Angew. Chem. Int. Ed*. 2016, **55**, 4194; b) S. Biswas, R. Mengji, S. Barman, V. Venugopal, A. Jana and N. D. P. Singh, *Chem. Commun*. 2018, **54**, 168.
13 X. Cheng, K. Wang, S. Huang, H. Zhang, H. Zhang and Y. Wang, *Angew. Chem. Int. Ed*. 2015, **54**, 8369.
14 B. Tang, H. Liu, F. Li, Y. Wang and H. Zhang, *Chem. Commun*. 2016, **52**, 6577.
15 S. Park, J. E. Kwon, S.-Y. Park, O.-H. Kwon, J. K. Kim, S.-J. Yoon, J. W. Chung, D. R. Whang, S.-K. Park, D. K. Lee, D.-J. Jang, J. Gierschner and S. Y. Park, *Adv. Opt. Mater*. 2017, **5**, 1700353.
16 J. Massue, T. Pariat, P. M. Vérité, D. Jacquemin, M. Durko, T. Chtouki, L. Sznitko, J. Mysliwiec and G. Ulrich, *Nanomaterials*, 2019, **9**, 1093.
17 Z. Zhang, Y-A, Chen, W-Y. Hung, W-F. Tang, Y-H. Hsu, C-L. Chen, F-Y. Meng and P-T. Chou, *Chem. Mater*. 2016, **28**, 8815.
18 M. Mamada, K. Inada, T. Komino, W. J. Potscavage, Jr., H. Nakanotani, C. Adachi, *ACS, Cent. Sci*. 2017, **3**, 769.
19 K. Wu, T. Zhang, Z. Wang, L. Wang, L. Zhan, S. Gong, C. Zhong, Z-H. Lu, S. Zhan and C. Yang, *J. Am. Chem. Soc*. 2018, **140**, 8877.
20 B. Li, L. Zhou, H. Chen, Q. Huang, J. Lan, L. Zhou and J. You, *Chem. Sci*. 2018, **9**, 1213.
21 K. Skonieczny, J. Yoo, J. M. Larsen, E. M. Espinoza, M. Barbasiewicz, V. I. Vullev, C-H. Lee and D. T. Gryko, *Chem. Eur. J*. 2016, **22**, 7485.
22 J. Massue, A. Felouat, M. Curtil, P. M. Vérité, D. jacquemin, G. Ulrich, *Dyes and Pigments*, 2019, **160**, 915.
23 V. Trannoy, N. Guillou, C. Livage, C. Roch-Marchal, M. Haouas, A. Léaustic, C. Allain, G. Clavier, P. Yu and T. Devic, *Inorg. Chem*. 2019, **58**, 6918.
24 H. Bulska, *J. Lumin*. 1988, **39**, 293.
25 K. Rurack, U. Resch-Genger, W. Rettig, *J. Photochem. Photobio. A: Chem*. 1998, **118**, 143.
26 K. Rurack and R. Radeglia, *Eur. J. Inorg. Chem*. 2000, 2271.
27 K. Rurack, K. Hoffmann, W. Al-Soufi and U. Resch-Genger, *J. Phys. Chem. B* 2002, **106**, 9744.
28 M. Suresh, D. A. Jose and A. Das, *Org. Lett*. 2007, **9**, 441.
29 O. K. Abou-Zied, *J. Phys. Chem. B* 2010, **114**, 1069.
30 D. De, H. Kaur, A. Datta, *Chem. Asian J*. 2013, **8**, 728.
31 F. Plasser, M. Barbatti, A. J. A. Aquino and H. Lischka, *J. Phys. Chem. A* 2009, **113**, 8490.
32 N. Kundu, P. Banerjee, R. Dutta, S. Kundu, R. K. Saini, M. Halder and N. Sarkar, *Langmuir*, 2016, **32**, 13284.
33 L. Kaczmarek, B. Nowak, J. Zukowski, P. Borowicz, J. Sepiol and A. Grabowska, *J. Mol. Struct*. 1991, **248**, 189.
34 P. Borowicz, A. Grabowska, A. Les, L. Kaczmarek, B. Zagrodzki, *Chem. Phys. Lett*. 1998, **291**, 351.
35 L. Kaczmarek, B. Zagrodzki, B. Kamienski, M. Pietrzak, W. Schilf, A. Les, *J. Mol. Struct*. 2000, **553**, 61.
36 L. Kaczmarek, P. Borowicz, A. Grabowska, *J. Photochem. Photobio. A: Chem*. 2001, **138**, 159.
37 G. Ulrich, F. Nastasi, P. Retailleau, F. Puntoriero, R. Ziessel and S. Campagna, *Chem. Eur. J*. 2008, **14**, 4381.
38 A. Reynal, J. Etxebarria, N. Nieto, S. Serres, E. Palomares and A. Vidal-Ferran, *Eur. J. Inorg. Chem*. 2010, 1360.
39 L-Y. Liao, X-R. Kong and X-F. Duan, *J. Org. Chem*. 2014, **79**, 777.

View Article Online
DOI: 10.1039/D0NJ05600F

40 L. Lipkowski, A. Grabowska, J. Waluk, G. Calestani and B. A. Hess, Jr. *J. Crystallogr. Spectrosc. Res*. 1992, 22, 563.
41 L. H. Vogt, Jr. and J. G. Wirth, *J. Am. Chem. Soc*. 1971, **93**, 5402.